Journal of Materials Chemistry A

High-efficiency visible light-induced photoelectrocatalytic hydrogen production by CdS sensitized TiO2 nanorods on TiO2 nanotube arrays

Journal:	*Journal of Materials Chemistry A*
Manuscript ID	TA-ART-06-2015-004107.R2
Article Type:	Paper
Date Submitted by the Author:	14-Sep-2015
Complete List of Authors:	Yu, Jiangdong; Xiamen University, Gong, Cheng; Xiamen University, Wu, Zhi; Xiamen University, Sun, Lan; College of Chemistry and Chemical Engineering, Wu, Yongneng; Xiamen University, Xiao, Wang; Xiamen University, Su, Yufeng; Xiamen University, Lin, Changjian; Xiamen University, State Key Laboratory of Physical Chemistry of Solid Surfaces

Journal of Materials Chemistry A

Cite this: DOI: 10.1039/c0xx00000x

www.rsc.org/xxxxxx

PAPER

High-efficiency visible light-induced photoelectrocatalytic hydrogen production by CdS sensitized TiO_2 nanorods on TiO_2 nanotube arrays

Jiangdong Yu, Cheng Gong, Zhi Wu, Yongneng Wu, Wang Xiao, Yufeng Su, Lan Sun,* and Changjian Lin

Received (in XXX, XXX) Xth XXXXXXXXX 20XX, Accepted Xth XXXXXXXXX 20XX
DOI: 10.1039/c0xx00000x

A novel CdS/TiO_2 nanorods/TiO_2 nanotube arrays (CdS/TNRs/TNTs) photocatalyst was prepared. The self-organized highly oriented TiO_2 nanotube arrays (TNTs) were first synthesized by anodizing Ti sheet. The "flower-like" rutile TiO_2 nanorods (TNRs) were then grafted on the TNTs by a hydrothermal method. Subsequently, the CdS quantum dots (CdS QDs) were deposited on the surface of the resulting TNRs/TNTs using a sequential-chemical bath deposition (S-CBD) method. UV−vis diffuse reflectance spectra indicated that CdS/TNRs/TNTs sample showed the significantly enhanced absorption in the range from 350 to 700 nm. The photoelectrocatalytic hydrogen production activities of all samples were evaluated by using Na_2S and Na_2SO_3 as sacrificial reagents in water under a 300 W Xe lamp with a UV-light filter ($\lambda > 420$ nm). The results showed that CdS/TNRs/TNTs prepared by hydrothermal reaction for 4 h and S-CBD 15 cycles showed a hydrogen production rate approximately 14 times that of the TNTs. When compared to CdS/TNTs, CdS/TNRs/TNTs showed a 2.3 fold increase in hydrogen production, which can be attributed to the enlarged effective deposition area for CdS QDs by depositing "flower-like" rutile TiO_2 nanorods on the TNTs. In addition, CdS/TNRs/TNTs exhibited the excellent hydrogen production stability using Na_2S and Na_2SO_3 as sacrificial reagents.

1. Introduction

As a kind of clean and storable high-energy capacity fuel, hydrogen has been recognized as a promising energy source. Since the abundant solar energy can be converted into hydrogen energy by using photocatalysts in reasonably designed photoelectrochemical cells (PECs),[1,2] the hydrogen production by PECs water splitting has become one of the reliable and efficient ways to solve the problem of energy shortage in the future.[3,4] The key in PECs is the photocatalysts, and thus finding a suitable photocatalyst has attracted many researchers' attention. Since Fujishima and Honda reported the discovery of photocatalytic water splitting on TiO_2 electrodes in 1972,[5] TiO_2 has always been regarded as the most promising material as photoanode. Among various TiO_2 nanostructures, highly ordered TiO_2 nanotube arrays (TNTs) has attracted tremendous attention due to its superior mechanical property, high specific surface area and rapid electron transmission.[6-8] However, TiO_2-based photoanodes always suffer from poor absorption of visible light in the solar spectrum due to the large band gap (i.e., ~3.2 eV for anatase; ~3.0 eV for rutile). To this end, many strategies, including doping with other elements and sensitizing with narrow band gap semiconductors, have been employed to modify the photoanodes' properties for optimizing the use of solar energy.

Focusing on sensitization strategy, the metal chalcogenides with narrow band gaps have been extensively studied and regarded as good candidates for visible-light-driven photocatalysts. Of particular interest among them is CdS with a direct band gap of 2.4 eV which matches well with the spectrum of sunlight and its conduction band edge is higher than that of TiO_2 facilitating the transfer of the photo-generated electrons at the interface between CdS and TiO_2. Coupling CdS with other wide band gap semiconductors such as TNTs and ZnO nanorods (ZnONRs) has been widely used in the fields of quantum dot (QD) sensitized solar cells,[9] visible-light-driven water splitting[10,11] and photocatalytic degradation of organic pollutants.[12] To date, CdS can be decorated on the Ti-based photoanodes through different methods such as electrochemical deposition,[13-15] sequential-chemical bath deposition (S-CBD),[16] successive ion-layer adsorption and reaction,[17] bifunctional organic linker method[18] and layer-by-layer assembly.[19] Among these methods, the S-CBD is a convenient and simple one, but the CdS QDs mostly deposited on the tube mouth of the TNTs as it is hard for Cd^{2+} and S^{2-} to permeate into nanotubes. It should be further noted that the very limited amount of CdS QDs handicaps the photoanode's absorption of visible light.[12] Therefore, introducing a compact oxide layer as the substrate for CdS QDs can not only preserve the one-dimensional nanotube arrays' desirable property providing direct electron pathways but also enlarge the effective deposition area of CdS QDs.[20] It has been demonstrated that TiO_2NTA/ZnONRs/CdS composite

photocatalyst synthesized has the increased hydrogen production rate.[21]

Herein, we present a CdS/TNRs/TNTs photocatalyst by a two-step process, where flower-shaped rutile TNRs were first grafted on TNTs through a simple hydrothermal method and then CdS QDs were deposited on TNRs/TNTs using S-CBD method. The photoelectrochemical performance and photoelectrocatalytic hydrogen production of the as-prepared CdS/TNRs/TNTs under visible light irradiation were investigated in aqueous solution containing Na_2S and Na_2SO_3 and compared with those of TNTs, TNRs/TNTs and CdS/TNTs.

2. Experimental Section

2.1. Preparation of the CdS/TNRs/TNTs heterostructures

Fig. 1 illustrates the synthesis procedure of CdS/TNRs/TNTs samples. Ti foil (purity > 99 %) with a thickness of 0.1 mm was cut into pieces of 1.5 cm × 1 cm. The highly organized and vertically oriented TNTs were fabricated by electrochemical anodization. Prior to the anodization, the Ti foils were cleaned in acetone, alcohol and distilled water using an ultrasonic bath for 15 min sequentially. The cleaned Ti foils were then immersed in an aqueous solution containing 0.5% wt HF at room temperature and anodized at 20 V for 30 min in a two-electrode cell with Ti foil as the working electrode and Pt foil as the counter electrode. Subsequently, the samples were thoroughly rinsed with deionized water and dried in air. In order to form the crystalline anatase TiO_2, the resulting amorphous TNTs were annealed at 450 ^oC for 2 h with heating rates of 5 ^oC min^{-1} and then cooled to room temperature naturally.

The "flower-like" TNRs were grafted on TNTs through a simple hydrothermal route. Briefly, 0.4 mL $TiCl_3$ and 0.8 mL HCl were added into 50 mL distilled H_2O. After stirred vigorously for 15 min, the mixture solution and TNTs were transferred into a Teflon-lined stainless steel autoclave. The hydrothermal process was conducted at 80 ^oC for a desired time and then the autoclave was cooled to room temperature naturally.

CdS QDs were deposited on the surface of TNRs/TNTs by S-CBD. Typically, the TNRs/TNTs were immersed successively in 0.05 M $CdCl_2$ aqueous solution and 0.05 M Na_2S aqueous solution for 30 s. Between each immersion step, the samples were rinsed with deionized water adequately to remove excess ions in the nanotube arrays. Such immersion cycle was repeated for up to 20 cycles. After finishing the coating, the samples were rinsed with deionized water. Finally, the samples were annealed at 450 ^oC for 2 h with heating rates of 5 ^oC min^{-1} and then cooled to room temperature naturally. For comparison, CdS QDs were also deposited on the surface of TNTs and TNRs under following the afore-mentioned procedure.

2.2. Materials characterization

The morphology of the samples was examined using a field emission scanning electron microscope (FE-SEM) (Hitachi S4800). The crystalline structure was identified by transmission electron microscopy (TEM) (JEM 2100) and X-ray diffraction (XRD) (Phillips, Panalytical X'pert, Cu Kα radiation (λ = 1.5417 Å)). The composition of the samples was analyzed by X-ray photoelectron spectroscopy (XPS, VG. Physical Electrons Quantum 2000 Scanning Esca Microprob, Al Kα radiation). The binding energies were calibrated to the signal for adventitious C 1s at 284.8 eV. UV-visible diffuse reflectance spectra (DRS) of the samples were recorded by a UV-vis-NIR spectrophotometer (Varian Cary 5000)

.

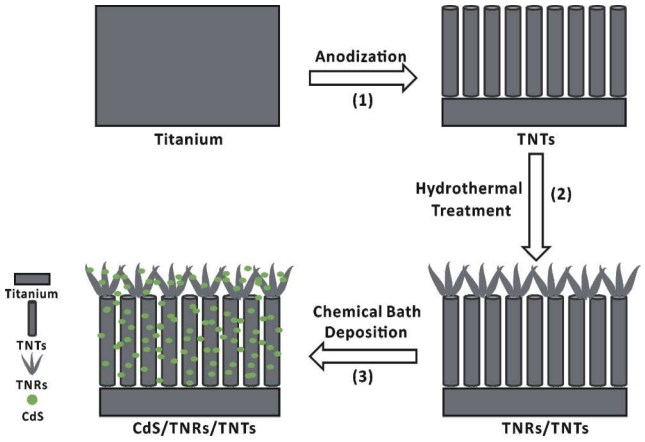

Fig. 1. Schematic diagram for the synthesis of CdS/TNRs/TNTs photoanode.

2.3. Photoelectrochemical performance and photoelectrocatalytic hydrogen production activity

The photocurrent measurements were carried out in a 3-arm cell with a quartz window and 1 M Na_2S was used as the electrolyte solution. The three-electrode configuration composed of the various samples as working electrodes, Pt wire as a counter electrode, and an Ag/AgCl as a reference electrode. The photocurrent under different wavelength of incident light irradiation was measured using LPX150 Xe lamp and SBP300 grating spectrometer (Beijing Zolix, China), and Model 163A potentiostat, Model 194 wave chopper, Model 5210 phase-locked amplifier (AMETEK Inc.). Photocurrent density-potential (J-V) characteristics were recorded using Ivium EC portable analyzer. A 300 W Xe lamp (PLS-SXE300, Beijing Bofeilai Technology Co, Ltd.) with a UV-light filter (λ > 420 nm) was employed as the light source. Electrochemical impedance spectroscopy (EIS) spectra were measured by applying an AC voltage of 2 mV amplitude within the frequency range of 10^5-10^{-1} Hz in 0.25 M Na_2S and 0.35 M Na_2SO_3 mixing solution with a sample as a working electrode, Pt wire as a counter electrode, and the saturated calomel electrode (SCE) as a reference electrode. The open circuit potential applied to the working electrode is 0 V (vs. SCE).

To evaluate the photocatalytic performance, the water splitting experiment was carried out in a gas-closed circulation system equipped with a three-electrode photoelectrochemical (PCE) cell and a volumetric device with a vacuum line. The electrolyte was a mixing solution of 0.25 M Na_2S and 0.35 M Na_2SO_3. The electrolyte was purged with N_2 for 30 min to remove O_2 prior to the experiment. A 300 W Xe lamp with a UV-light filter (λ > 420 nm) was used as a solar light source with a light intensity of 320 $mW \cdot cm^{-2}$. The irradiation area for all samples was 1 cm^2.

3. Results and Discussion

3.1. Morphological characterization

Fig. 2a-f show the SEM top-view and cross-sectional images of TNTs, TNRs/TNTs and CdS/TNRs/TNTs prepared by hydrothermal reaction for 4 h and 15 S-CBD cycles, respectively. The self-organized TiO_2 layer consisted of vertically aligned compact nanotube arrays with an average tube diameter of about 90 nm (Fig. 2a) and an average length of 380 nm (Fig. 2b). After TNTs was treated by a hydrothermal process in a mixing solution containing $TiCl_3$ and HCl at 80 ^oC for 4 h, the "flower-like" TNRs were grafted on the nozzles of the TiO_2 nanotubes (Fig. 2c and d). As the petals overlapping each other, there were large amount of interstices in the TiO_2 nanorod layer. Moreover, some mouths of the TiO_2 nanotubes could still be seen clearly beneath the flowers. Compared with pure TNTs, this new hierarchically structure has an even larger effective surface area, which is beneficial to achieve a higher dispersion of CdS QDs. Further treatment of TNRs/TNTs using S-CBD approach led to form a thin CdS coating on the TNRs/TNTs. It is not easy to identify CdS QDs on the surface due to very small size,[22] but The surface of TNRs/TNTs became rough, and the "petals" turned thicker (Fig. 2e), indicating that many CdS QDs were deposited on the "flower-like" TiO_2 nanorods. However, few CdS QDs can be observed inside the TiO_2 nanotubes because many TNRs covered the mouth of the nanotubes (Fig. 2f). CdS QDs were also deposited on TNTs under the same conditions for reference, as shown in Fig. 2g and h. Some CdS QDs were deposited on the surface of TNTs (inset of Fig. 2g) and only a few CdS QDs can be found inside the TiO_2 nanotubes.

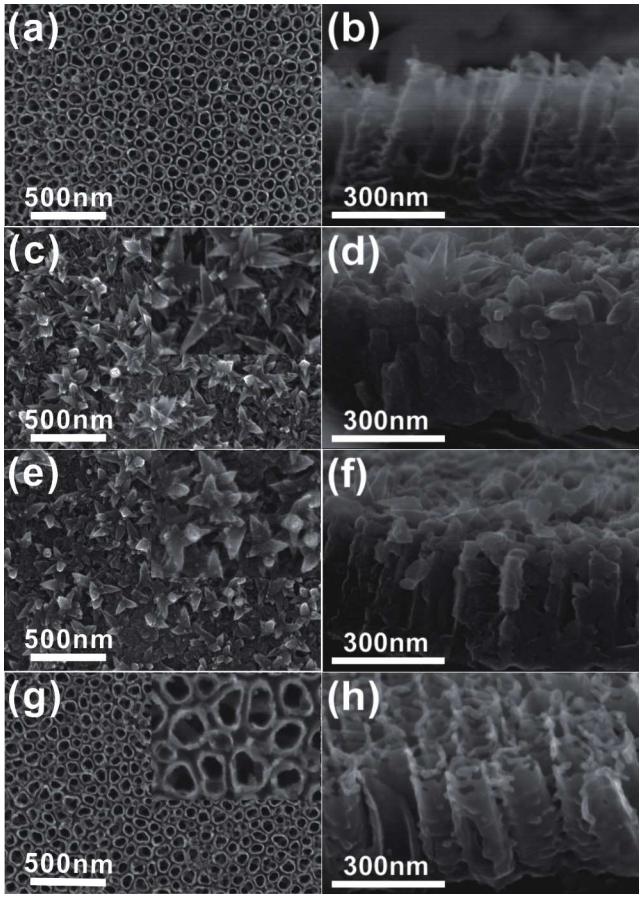

Fig. 2. SEM images of (a, b) TNTs, (c, d) TNRs/TNTs, (e, f) CdS/TNRs/TNTs and (g, h) CdS/TNTs.

3.2. Crystalline structure characterization

To identify the CdS/TNRs/TNTs structure, the morphology of CdS/TNRs/TNTs prepared by hydrothermal reaction for 4 h and 15 S-CBD cycles was further examined by TEM and HRTEM. Fig. 3a shows a low magnification TEM image of as-fabricated CdS/TNRs/TNTs sample. Its film thickness was about 760 nm. Fig. 3b presents a high magnification TEM image of as-fabricated CdS/TNRs/TNTs sample taken the upper edge of TNTs. The inner pore diameter and wall thickness of TiO_2 nanotubes were about 56 nm and 16 nm, respectively. A TEM image of the CdS/TNRs is presented in Fig. 3c. The CdS QDs were dispersed homogeneously on the surface of TNRs. The selected area energy diffraction (SAED) pattern shown in inset of Fig. 3c demonstrated that the TNRs deposited on the surface of TNTs was rutile. Fig. 3d shows the HRTEM image obtained from a CdS/TiO_2 nanorod. The diameter of CdS QDs was determined to be about 9 nm. The high-resolution lattice image confirmed that the nanoparticle with an interplanar spacing of 0.336 nm (inset in Fig. 3d), which corresponds to the (220) plane of cubic CdS (JPCDS 80-0019). It can be concluded that the CdS QDs were successfully assembled on the rutile TNRs.

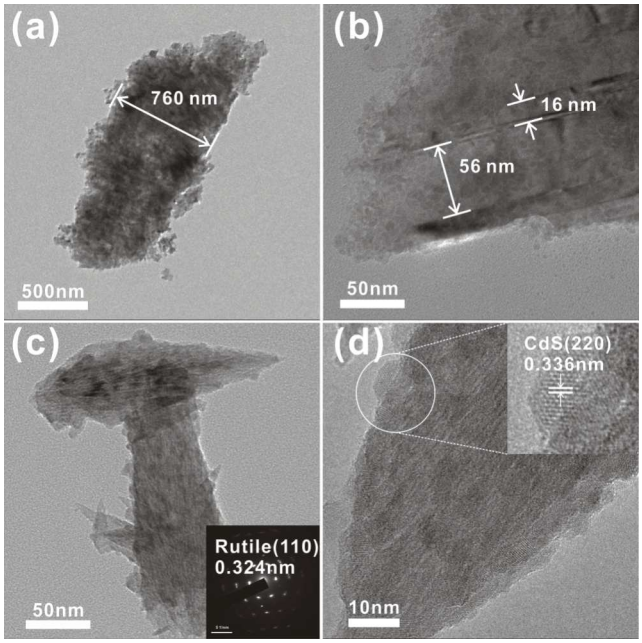

Fig. 3. TEM images of CdS/TNRs/TNTs: (a) Low-magnification of CdS/TNRs/TNTs, (b) High-magnification of CdS/TNRs/TNTs, (c) High-magnification of CdS/TNRs/TNTs and (d) HRTEM image of CdS/TNRs/TNTs. The insets in (c) and (d) show the SAED pattern of CdS/TNRs/TNTs and high magnification image of the marked area, respectively.

Fig. 4a shows XRD patterns of TNTs, TNRs/TNTs, CdS/TNTs and CdS/TNRs/TNTs. For TNTs, the diffraction peaks at $2\theta = 25.3°$ and 48.4° were attributed to the (101) and (200) crystal planes of anatase TiO_2. No diffraction peaks of rutile TiO_2 were observed, indicating that TNTs was pure anatase. Additional diffraction peak at $2\theta = 27.5°$ of rutile (110) appeared on TNRs/TNTs after hydrothermal treatment, indicating that the "flower-like" TNRs grafted on the anatase TNTs were rutile. It is worth noting that the CdS phase was not detected due to the

homogeneous dispersion and the low loading of CdS QDs on the surface of TNRs/TNTs.[23]

Considering CdS QDs can't be detected by XRD pattern, Raman spectra were employed to identify the existence of CdS QDs due to its strong Raman characteristic signals. As shown in Fig. 4b, TNTs sample displayed anatase. Four peaks at 149, 400, 519 and 637 cm^{-1} could be assigned to the Raman active modes *Eg*(1), *B1g*(1), *B1g*(1) and *Eg*(3) of anatase TiO_2, respectively. TNRs/TNTs sample demonstrated a mixture of anatase and rutile. The characteristic vibrations of bulk rutile TNRs was faintly observed at 448 cm^{-1} because the surface scattering dominated the Raman spectra of rutile TNRs rather than the volume scattering, suggesting that the grafted TNRs layer is very thin and has high surface-to volume ratio.[24] For CdS/TNTs and CdS/TNRs/TNTs, two additional peaks were detected. The peak at 305 cm^{-1} was ascribed to the longitudinal optical (1LO) phonon mode of CdS and the other peak at 605 cm^{-1} was due to its overtone (2LO) mode, indicating the formation of CdS on TNTs and TNRs. The relatively narrow peaks of CdS may correspond to the relatively small amount, which was in agreement with the SEM and XRD pattern.

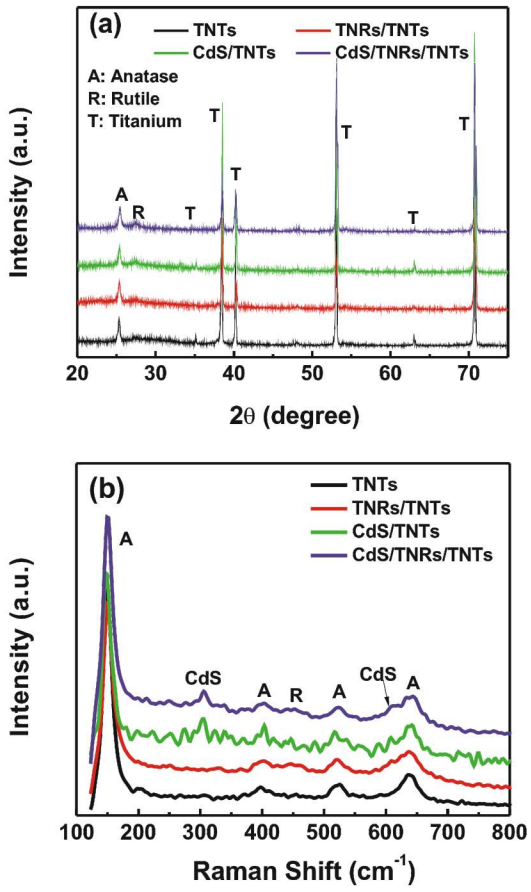

Fig. 4. (a) XRD patterns and (b) Raman spectra of TNTs, TNRs/TNTs, CdS/TNTs and CdS/TNRs/TNTs.

XPS measurements were performed to further investigate the surface chemical composition and oxidation state of CdS/TNRs/TNTs film. Fig. 5a shows XPS survey spectrum of CdS/TNRs/TNTs sample prepared by hydrothermal reaction for 4 h and 15 S-CBD cycles. The characteristic peaks of Ti 2p, O 1s, Cd 3p, Cd 3d, S 2s, S 2p and C 1s can be clearly identified. The C element can be attributed to the trace hydrocarbon from XPS instrument itself. High-resolution XPS of the O element is shown in Fig. 5b. The strong peak at 529.87 eV can be assigned to the anionic oxygen in TiO_2 lattice,[25] and the small peak at 531.43 eV can be attributed to the oxygen in a surface hydroxyl.[26,27] Fig. 5c and d present the XPS spectra of Cd and S elements, respectively.

The binding energies of Cd $3d_{3/2}$ and Cd $3d_{5/2}$ were located at 411.85 eV and 405.18 eV, respectively. The 6.7 eV difference between the binding energies of Cd $3d_{3/2}$ and Cd $3d_{5/2}$ peaks was a characteristic of Cd^{2+} states.[28] The S 2p signal was divided into two different peaks. The peak at 161.88 eV could be ascribed to the S^{2-} anion, and the other one at 168.70 eV could be assigned to the oxidized SO_3^{2-} or SO_4^{2-} form,[29] indicating that the deposited CdS QDs were partly oxidized.

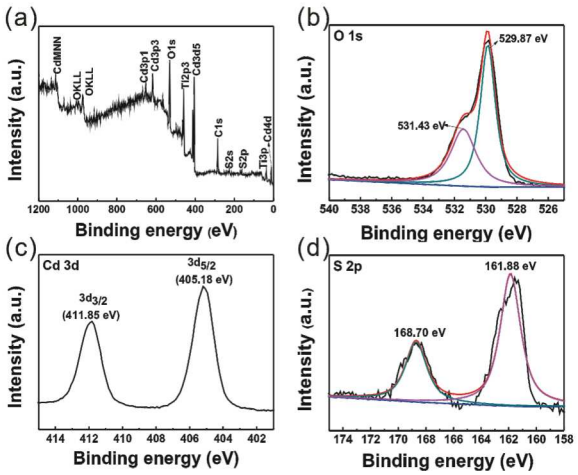

Fig. 5. XPS spectra of CdS/TNRs/TNTs: (a) survey XPS spectrum and high resolution spectra of O 1s (b), Cd 3d (c) and S 2p (d).

3.3. UV-vis diffuse reflectance spectra

Fig. 6a shows the UV-vis DRS of TNTs, TNRs/TNTs, CdS/TNRs/TNTs prepared by hydrothermal reaction for 4 h and 15 S-CBD cycles and CdS/TNTs prepared by 15 S-CBD cycles. The absorption onset of TNTs was at approximately 390 nm, which is in line with the band gap of anatase TiO_2 (3.2 eV). The absorption of TNTs in visible region could be assigned to the sub-bandgap states of the TNTs.[30] Fig. 6b is the $(\alpha hv)^{1/2}$-hv curve coming from the equation $(\alpha hv)^2=k(hv - E_g)$, where α, h, v and E_g represent adsorption coefficient, Planck constant, light frequency and band energy, respectively.[31] Compare with TNTs, the absorption band edge of TNRs/TNTs showed a slight red shift, as the band gap of rutile is 3.0 eV less than anatase's. After the deposition of CdS QDs on the TNTs, the absorption band edge of the sample was shifted towards more the visible-light region and thus the band gap dramatically decreased from 3.0 eV to 2.4 eV as a result of the small band gap of CdS (2.4 eV) which can be excited under visible light irradiation. Intriguingly, for CdS/TNRs/TNTs, the visible light absorption was progressively enhanced and entirely covered the CdS/TNTs absorption. Therefore, CdS/TNRs/TNTs is respected to have higher

photocatalytic activity than TNTs, TNRs/TNTs and CdS/TNTs under visible light irradiation.

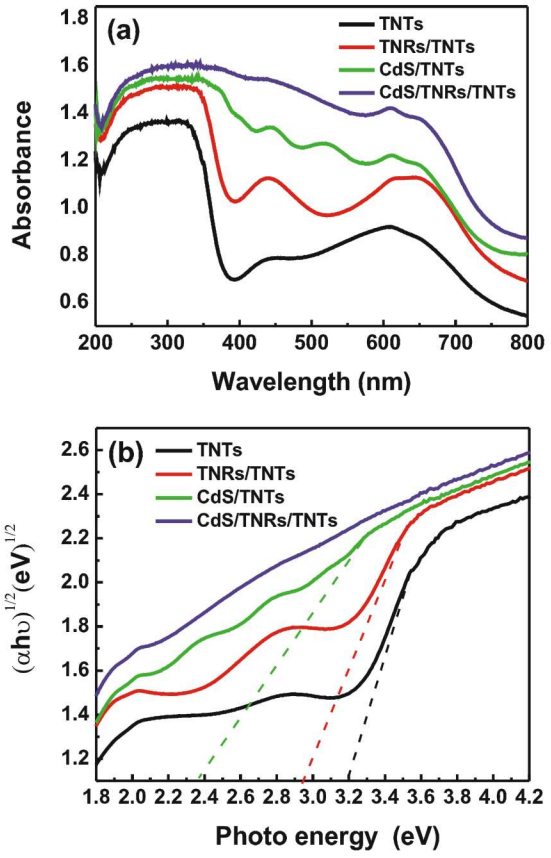

Fig. 6. (a) UV-vis diffuse reflectance absorption spectra and (b) the absorption spectra of the by plotting $(\alpha hv)^{1/2}$ vs. hv of TNTs, TNRs/TNTs, CdS/TNTs and CdS/TNRs/TNTs.

3.4. Photoelectrochemical performance

The photocurrent reflects the reduction of the recombination rate of photogenerated electron-hole pairs and the photoexcited electron transfer efficiency. In order to obtain the CdS/TNRs/TNTs sample with the highest photocurrent response, the effects of hydrothermal times and S-CBD cycle times on photocurrent density of CdS/TNRs/TNTs were examined. Fig. S1A shows the SEM images of CdS/TNRs/TNTs prepared by different hydrothermal times and 15 S-CBD cycles. As the hydrothermal time increased from 2 h to 4 h, the surface of TNTs was gradually covered by TNRs. When the hydrothermal time increased to 8 h, the TNRs agglomerated together into a dense film. Fig. S1B presents the corresponding photocurrent density-time characteristics at a - 0.5 V bias vs. SCE with a pulse of 50 s under visible light irradiation. The photocurrent densities of CdS/TNRs/TNTs increased first and then decreased with an increase of TNRs loading, suggesting that the amount of TNRs can be readily optimized. The highest steady photocurrent density (2.41 mA·cm^{-2}) was achieved from 4 h hydrothermal deposition sample. When the hydrothermal time was increased to 8 h, the photocurrent density sharply dropped to 0.36 mA·cm^{-2}. Combined with the observation in Fig. S1A, the great decrease of photocurrent density was due to the dense rutile film which was adverse to the deposition of CdS QDs. In addition, the carriers recombined severely in this kind of dense film. Fig. S2 shows photocurrent density-time characteristics of CdS/TNRs/TNTs prepared by hydrothermal reaction for 4 h and different S-CBD cycles. As the amount of CdS increased upon increasing the S-CBD cycles to 15, the photocurrent density increased to a maximum of 2.41 mA·cm^{-2}. However, when the S-CBD cycles were further increased to 20, the photocurrent density decreased to 1.89 mA·cm^{-2} due to the aggregation of CdS crystallites, leading to the increase of the recombination rate of photogenerated electron-hole pairs.

Fig. 7 shows photocurrent densities of TNTs, TNRs/TNTs, CdS/TNTs and CdS/TNRs/TNTs prepared by hydrothermal reaction for 4 h and S-CBD 15 cycles (i.e., the sample possessing the highest photocurrent density) under continuous monochromatic light irradiation in an aqueous solution containing 1 M Na_2S. All electrodes exhibited a photocurrent response peak around 345 nm. The maximum photocurrent density for TNTs is 686.8 nA·cm^{-2}. After grafting with TNRs, the photocurrent density of TNRs/TNTs was increased, yielding a maximum photocurrent density of 1240.0 nA·cm^{-2} due to the formation of heterojunctions between anatase and rutile TiO_2 which reduced the recombination of charge carrier[20,32] and larger effective contact area between hierarchically structured TNRs/TNTs and electrolyte. As expected, both TNTs and TNRs/TNTs show rather poor photocurrent response in visible region. Compared with TNTs, the photocurrent response of CdS/TNTs can be extended to visible region (~ 490 nm), which can be ascribed to the narrow band gap of CdS (2.4 eV). Depositing CdS QDs on TNRs/TNTs further improved the photocurrent response in both UV and visible light region, implying decreased electron-hole recombination and improved charge separation.

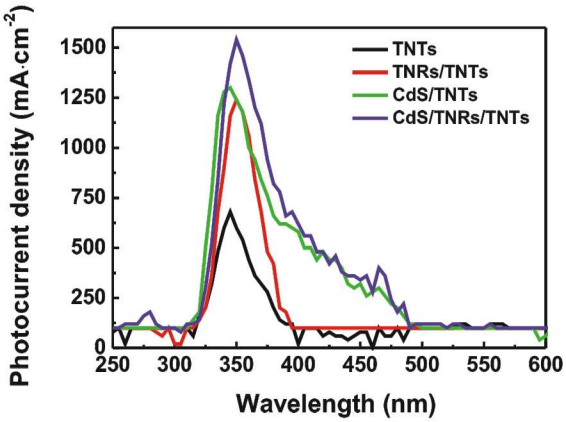

Fig. 7. Photocurrent spectra of TNTs, TNRs/TNTs, CdS/TNTs and CdS/TNRs/TNTs.

The effect of applied potential on the photocurrent response was also investigated by potentiodynamic scans in a three-electrode configured photoelectrochemical cell. Fig. 8a shows the photocurrent densities of TNTs, TNRs/TNTs, CdS/TNTs and CdS/TNRs/TNTs prepared by hydrothermal reaction for 4 h and S-CBD 15 cycles under visible light irradiation as the function of

applied potential. The photocurrent of both TNTs and TNRs/TNTs electrodes was negligible. After the CdS QDs were

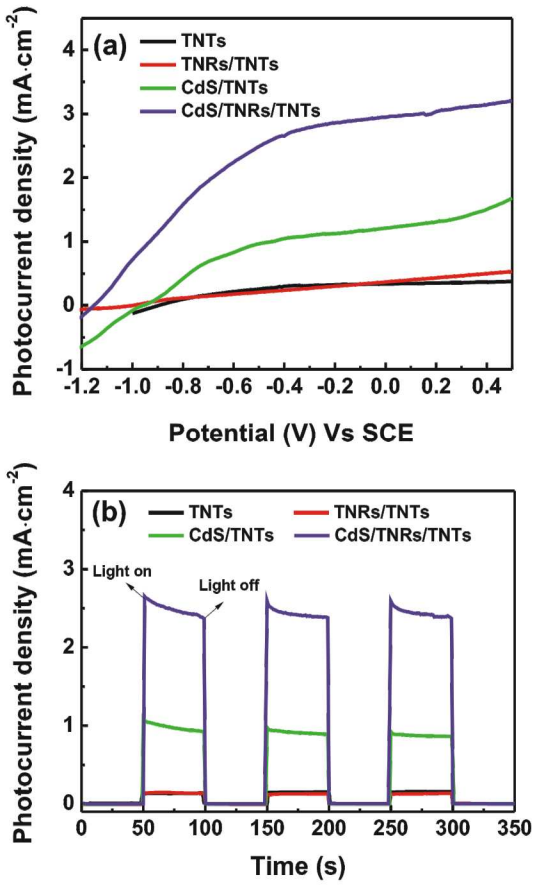

Fig. 8. (a) J-V and (b) J-t (a bias of - 0.5 V (Vs SCE)) curves of TNTs, TNRs/TNTs, CdS/TNTs and CdS/TNRs/TNTs under visible light irradiation.

directly deposited on TNTs, the photocurrent density of TNTs raised with the increase of bias potential ranging from - 1.2 V to 0.5 V vs. SCE. In particular, when CdS QDs were deposited on TNRs/TNTs electrode, the photocurrent density increased remarkably, and the saturated photocurrent density of CdS/TNRs/TNTs (2.49 mA·cm^{-2}) was approximately 18 times that of pure TNTs (0.14 mA·cm^{-2}) at - 0.5 V. It is obvious that the effect of CdS is more prominent in the CdS/TNRs/TNTs system, as the result of the improved distribution of the CdS QDs and the effective separation of the photogenerated charges which is essential for high-efficiency photoelectrocatalytic hydrogen production.[33,34] In order to further clarify the effect the heterojunctions between ruitle TNRs and anatase TNTs, the SEM and photocurrent density of CdS/TNRs in which TNRs grew on the surface of pure Ti foil were shown in Fig. S3, respectively. The flower-like TNRs can be observed. Interestingly, the photocurrent density of CdS/TNRs was twice as much as that of CdS/TNTs, which is attributed to the larger amount of CdS deposited on CdS/TNRs, while the photocurrent density of CdS/TNRs/TNTs was higher than that of CdS/TNRs, indicating that the heterojunctions between TNRs and TNTs promoted the separation of photogenerated electrons and holes. Notably, the deposition of CdS also conduced to the negative shift of flat band potential, indicating a shift in Fermi level of the TiO_2-CdS heterostructure to more negative potential.[35] This confirms that CdS QDs deposited on TNRs/TNTs can prolong the lifetime of the photogenerated carriers.[36]

Fig. 8b shows the photocurrent density-time characteristics of TNTs, TNRs/TNTs, CdS/TNTs and CdS/TNRs/TNTs at a - 0.5 V bias vs. SCE with a pulse of 50 s under visible light irradiation. All the samples showed an instantaneous rise in photocurrent which retained a steady-state value during the entire illumination period, while the photocurrent retracted to original values as soon as the light turned off. The photocurrent densities of TNTs and TNRs/TNTs were about the same value (0.14 mA·cm^{-2}). Compared with TNTs, the photocurrent densities of CdS/TNTs (0.91 mA·cm^{-2}) and CdS/TNRs/TNTs (2.41 mA·cm^{-2}) increased 6.7 and 17 fold, respectively. This result further indicates that CdS depositing significantly improves the photocurrent as the electron photo-generated in CdS can rapidly migrate toward the TiO_2 nanotubes, which effectively prevents the electron-hole pairs from recombining. Moreover, this improvement is more effective when the CdS was deposited on the grafted TNRs, as this construction provide larger amount of CdS QDs.

As a widely used electrochemical method, EIS is very effective tool to investigate the electron-transfer properties of the interface between electrodes and solution. The less impedance arc radius in Nyquist plots implys the faster electron transfer. Fig. 9 shows the EIS of TNTs, TNRs/TNTs, CdS/TNRs/TNTs prepared by hydrothermal reaction for 4 h and 15 S-CBD cycles and CdS/TNTs prepared by 15 S-CBD cycles under visible irradaition. The TNTs exhibited almost a straight line which represents the characteristics of diffusion limited electron-transfer process on the electrode surface. Comparatively, the TNRs/TNTs showed a smaller depressed semicircle arc. This means that the interfacial charges can transfer more rapidly and induce effective separation of photogenerated electrons and holes. Clearly, the diameter of the semicircle of CdS/TNRs/TNTs was smaller than that of CdS/TNTs, demonstrating that the TNRs/TNTs heterojunctions improved the separation of photogenerated electrons and holes, which is in good agreement with the photocurrent measurements.

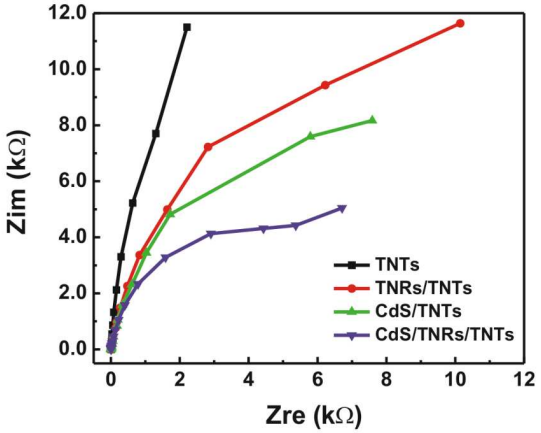

Fig. 9. EIS patterns of TNTs, TNRs/TNTs, CdS/TNTs and CdS/TNRs/TNTs.

3.5. Photoelectrocatalytic hydrogen production activity

The different photoanodes were used for photoelectrocatalytic H_2 generation under visible-light irradiation using Na_2S/Na_2SO_3 as a scavenging agent at - 0.5 V. Fig. 10a shows the hydrogen production rates of TNTs, TNRs/TNTs, CdS/TNTs and CdS/TNRs/TNTs as photoanodes for photoelectrocatalytic water splitting for 1 h. It is not surprising that, in line with the photocurrent results, both the TNTs and TNRs/TNTs exhibited a very low photocatalytic activity, and the hydrogen production rate was 1.78 $\mu mol \cdot h^{-1} \cdot cm^{-2}$ and 1.85 $\mu mol \cdot h^{-1} \cdot cm^{-2}$, respectively. After depositing CdS QDs on TNTs, the photocatalytic activity of CdS/TNTs was effectively improved with a hydrogen generation rate of 10.68 $\mu mol \cdot h^{-1} \cdot cm^{-2}$. The photocatalytic activity further increased when the CdS QDs were deposited on TNRs/TNTs, and the corresponding average hydrogen production rate was 24.74 $\mu mol \cdot h^{-1} \cdot cm^{-2}$, which is 14 times that of TNTs. The stability of CdS/TNRs/TNTs was also estimated. Fig. 10b shows the amount of H_2 produced by CdS/TNRs/TNTs photoanode in 1 h during a series of 5 identical tests. The amount of H_2 production decreased only 5.9 % after 5 h irradiation. These results indicated that the CdS/TNRs/TNTs electrode was relatively high active and stable to generate H_2 for a long period of time.

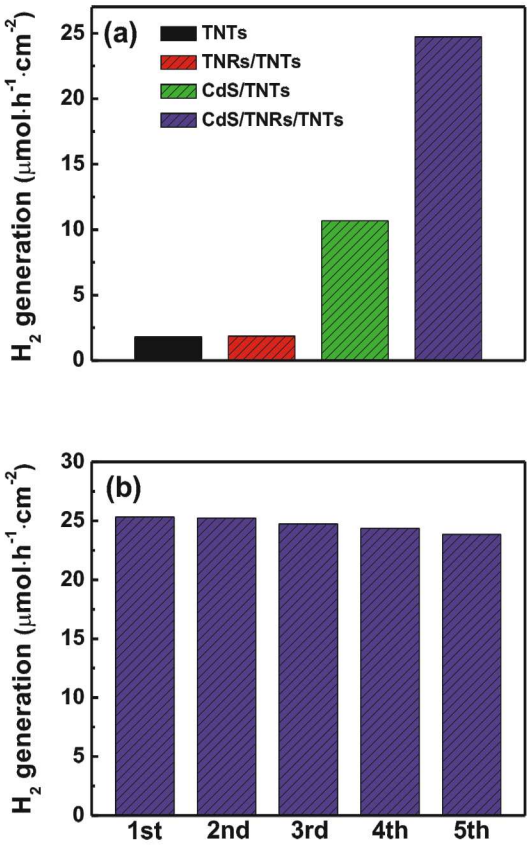

Fig. 10. (a) The hydrogen production rates on different photoanodes and (b) the reusability of CdS/TNRs/TNTs.

Fig. 11 clearly elucidate the feasibility of the intersystem injection of excited electrons from CdS to TiO_2. The pristine TiO_2 could barely absorb visible light to produce electrons due to the large band gap. Under visible light irradiation, the electrons in the valence band (VB) of CdS are excited to its conduction band (CB). Since the CB of bulk CdS is more negative than that of TiO_2, the photogenerated electrons from the CdS QDs can quickly inject to the TiO_2. Notably, the flat band position of the rutile TiO_2 is about 0.05 V positive than that of anatase TiO_2 and the Fermi level of the anatase is more close to the CB position,[32] and thus the photogenerated electrons in the CB of TNRs (rutile) can transfer to the CB of TNTs (anatase) and are collected at TNTs electrode, subsequently transfer to the external circuit. Meanwhile, the photogenerated holes accumulated at the VB of CdS are responsible for the electron donors, which protect CdS from self-photocorrosion under irradiation.[37] Since the photoanode and Pt counter electrode constitute a circuit, the photogenerated electrons are ultimately transferred to Pt wire and subsequently scavenged by hydrogen ion, forming hydrogen gas. The presence of the TNTs and TNRs could provide a rapid transmission channel for the photogenerated electrons. Thus, CdS QDs can be regarded as photosensitizer because they absorb visible light and generate photogenerated electrons that transfer to the CB of TiO_2, while the holes which accumulated at the VB of CdS can be effectively depleted by the Na_2S/Na_2SO_3 sacrificial reagents. This scenario not only favors the separation of photogenerated electrons and holes but also depresses the photocorrosion of CdS. The major reactions that occur in this system can be summarized as follows:[38,39]

Pt counter electrode:

$$2H^+ + e^- \rightarrow H_2 \quad (1)$$

CdS/TNRs/TNTs photoanode:

$$2S^{2-} + 2h_{vb}^+ \rightarrow S_2^{2-} \quad (2)$$

$$S_2^{2-} + SO_3^{2-} \rightarrow S_2O_3^{2-} + S^{2-} \quad (3)$$

$$S^{2-} + SO_3^{2-} + 2h_{vb}^+ \rightarrow S_2O_3^{2-} \quad (4)$$

$$SO_3^{2-} + 2OH^- + 2h_{vb}^+ \rightarrow SO_4^{2-} + H_2O \quad (5)$$

$$2SO_3^{2-} + 2h_{vb}^+ \rightarrow S_2O_6^{2-} \quad (6)$$

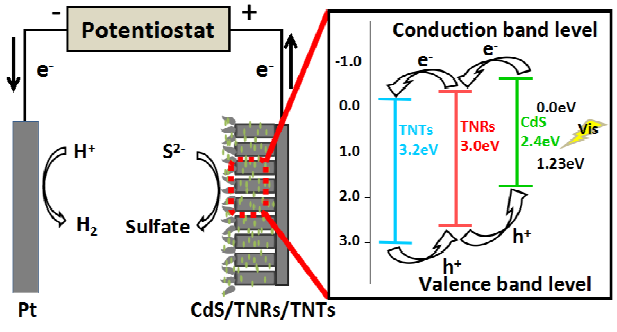

Fig. 11. Schematic diagram of photoelectrocatalytic process on CdS/TNRs/TNTs

With effective charge separation, the photogenerated electrons have long enough lifetime to reduce H^+ to H_2, and using electron

donors as sacrificial agents improve the stability of the photoanode.

4. Conclusion

The CdS/TNRs/TNTs composite photocatalyst was successfully fabricated by combing the hydrothermal method with the S-CBD. It was demonstrated that the optimal photocatalyst has a high efficiency of hydrogen production by water splitting in a solution containing Na_2S/Na_2SO_3 sacrificial reagents under visible light irradiation. The potential gradient within the composite photocatalyst was beneficial to transfer photogenerated electrons from CdS QDs to TNTs, which could extend the lifetime of photogenerated electrons and further improve the efficiency of hydrogen production. Moreover, the presence of the "flower-like" rutile TNRs significantly improved the dispersion of CdS QDs. This work provides a facile synthesis of CdS/TNRs/TNTs composite photocatalyst which has potential application in visible-light-induced photoelectrocatalytic water splitting as a highly-efficient photoanode material.

Acknowledgements

This work was supported by the National Natural Science Foundation of China (21321062) and NFFTBS (J1310024).

Notes and references

State Key Laboratory of Physical Chemistry of Solid Surfaces, Department of Chemistry, College of Chemistry and Chemical Engineering, Xiamen University, Xiamen, 361005 (China). E-mail: sunlan@xmu.edu.cn

1. M. Grätzel, *Nature*, 2001, **414**, 338-344.
2. C. L. Tseng, C. J. Tseng and J. C. Chen, *Int. J. Hydrogen Energy*, 2010, **35**, 2781-2785.
3. M. Dresselhaus and I. Thomas, *Nature*, 2001, **414**, 332-337.
4. N. S. Lewis, *Nature*, 2001, **414**, 589-590.
5. A. Fujishima and K. Honda, *Nature*, 1972, **238**, 37-38.
6. S. Banerjee, S. K. Mohapatra, P. P. Das and M. Misra, *Chem. Mater.*, 2008, **20**, 6784-6791.
7. Y. Hou, X. Y. Li, Q. D. Zhao, X. Quan and G. H. Chen, *Adv. Funct. Mater.*, 2010, **20**, 2165-2174.
8. K. Xie, L. Sun, C. Wang, Y. Lai, M. Wang, H. Chen and C. Lin, *Electrochim. Acta*, 2010, **55**, 7211-7218.
9. W. Lee, S. K. Min, V. Dhas, S. B. Ogale and S. H. Han, *Electrochem. Commun.*, 2009, **11**, 103-106.
10. C. Li, J. Yuan, B. Han, L. Jiang and W. Shangguan, *Int. J. Hydrogen Energy*, 2010, **35**, 7073-7079.
11. P. Sheng, W. Li, J. Cai, X. Wang, X. Tong, Q. Cai, C.A. Grimes, *J. Mater. Chem. A*, 2013, **1**, 7806-7815.
12. Y. Xie, G. Ali, S. H. Yoo and S. O. Cho, *ACS Appl. Mater. Inter.*, 2010, **2**, 2910-2914.
13. S. Chen, M. Paulose, C. Ruan, G.K. Mor, O. K. Varghese, D. Kouzoudis and C.A. Grimes, *J. Photochem. Photobio. A: Chem.*, 2006, **177**, 177-184.
14. C. Wang, L. Sun, H. Yun, J. Li, Y. Lai and C. Lin, *Nanotechnology*, 2009, **20**, 295601.
15. Y. Yin, Z. Jin and F. Hou, *Nanotechnology*, 2007, **18**, 495608.
16. M. C. Hsu, I. C. Leu, Y. M. Sun and M. H. Hon, *J. Cryst. Growth*, 2005, **285**, 642-648.
17. Y. Lai, Z. Lin, D. Zheng, L. Chi, R. Du, C. Lin, *Electrochim. Acta*, 2012, **79**, 175-181.
18. J. ChuláKim, Y. BokáLee, J. HoonáHong, J. InáLee, J. WookáYang, W. InáLee and N. HwiáHur, *Chem, Commun.*, 2006, 5024-5026.
19. Y. G. Guo, J. S. Hu, H. P. Liang, L. J. Wan and C. L. Bai, *Adv. Funct. Mater.*, 2005, **15**, 196-202.
20. M. Ye, D. Zheng, M. Lv, C. Chen, C. Lin and Z. Lin, *Adv. Mater.*, 2013, **25**, 3039-3044.
21. L. Wu, J. Li, S. Zhang, L. Long, X. Li and C. Cen, *J. Phys. Chem. C*, 2013, **117**, 22591-22597.
22. S. Chaguetmi, F. Mammeri, M. Pasut, S. Nowak, H. Lecoq, P. Decorse, C. Costentin, S. Achour and S. Ammar, *J. Nanopart. Res.*, 2013, **15**, 1-10.
23. F. Su, J. Lu, Y. Tian, X. Ma and J. Gong, *Phys. Chem. Chem. Phys.*, 2013, **15**, 12026-12032.
24. S. T. Jostar, S. Devadason, J. Suthagar, *Mater. Sci. Semicond. Process.*, 2015, **34**, 65-73.
25. G. W. Simmons and B. C. Beard, *J. Phys. Chem. C*, 1987, **91**, 1143-1148.
26. K. E. Lee, M. A. Gomez, T. Regier, Y. Hu and G. P. Demopoulos, *J. Phys. Chem. C*, 2011, **115**, 5692-5707.
27. J. Singh, A. Gusain, V. Saxena, A. Chauhan, P. Veerender, S. Koiry, P. Jha, A. Jain, D. Aswal and S. Gupta, *J. Phys. Chem. C*, 2013, **117**, 21096-21104.
28. M. Kundu, A. Khosravi, S. Kulkarni and P. Singh, *J. Mater. Sci.*, 1997, **32**, 245-258.
29. K. Bandyopadhyay, K. Mayya, K. Vijayamohanan and M. Sastry, *J. Electron Spectrosc. Relat. Phenom.*, 1997, **87**, 101-107.
30. Y. Lai, L. Sun, Y. Chen, H. Zhuang, C. Lin and J. W. Chin, *J Electrochem. Soc*., 2006, **153**, D123-D127.
31. B. K. Vijayan, N. M. Dimitrijevic, J. Wu and K. A. Gray, *J. Phys. Chem. C*, 2010, **114**, 21262-21269.
32. P. Yan, X. Wang, X. Zheng, R. Li, J. Han, J. Shi, A. Li, Y. Gan, C. Li, *Nano Energy*, 2015, **15**, 406-412.
33. M. Ye, J. Gong, Y. Lai, C. Lin, Z. Lin, *J. Amer. Chem. Soc.*, 2012, **134**, 15720-15723.
34. Y. Lai, J. Gong, C. Lin, *Int. J. Hydrogen Energy*, 2012, **37**, 6438-6446.
35. J. Luo, L. Ma, T. He, C. F. Ng, S. Wang, H. Sun and H. J. Fan, *J. Phys. Chem. C*, 2012, **116**, 11956-11963.
36. L. Sun, J. Cai, Q. Wu, P. Huang, Y. Su and C. Lin, *Electrochim. Acta*, 2013, **108**, 525-531.
37. R. Williams, *J Chem. Phys.*, 1960, **32**, 1505-1514.
38. H. Park, W. Choi and M. R. Hoffmann, *J. Mater. Chem.*, 2008, **18**, 2379-2385.
39. J. F. Reber and M. Rusek, *J. Phys. Chem.*, 1986, **90**, 824-834.

Graphical Abstract

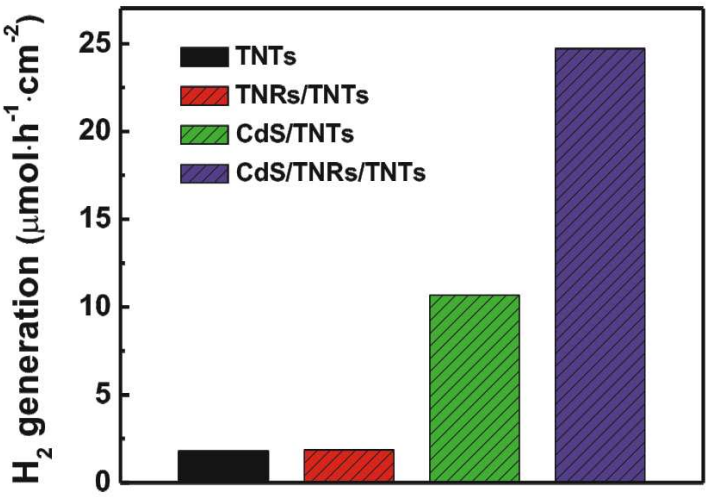

CdS/TNRs/TNTs were synthesized by combing the hydrothermal method with the sequential-chemical bath deposition method and displayed the effectively enhanced photoelectrocatalytic hydrogen production activity under visible light irradiation compared with TNTs, TNRs/TNTs and CdS/ TNTs.